

ITO-less silicon heterojunction solar cells based on nanocrystalline silicon carrier collectors



Yuxiang Li ^{b,1}, Yubo Zhang ^{c,1}, Xuejiao Wang ^{a,d,e,f,g}, Jilei Wang ^h, Guanlan Chen ^{a,d,e,f,g}, Biao Shi ^{a,d,e,f,g}, Liyou Yang ^h, Wenhong Wang ^b, Ying Zhao ^{a,d,e,f,g,*}, Xiaodan Zhang ^{a,d,e,f,g,**}

^a Institute of Photoelectronic Thin Film Devices and Technology, State Key Laboratory of Photovoltaic Materials and Cells, Nankai University, Tianjin, 300350, PR China

^b School of Electronic and Information Engineering, Tiangong University, Tianjin, 300387, PR China

^c Tianjin Port Information Technology Development Co., Ltd, Tianjin, 300450, PR China

^d Key Laboratory of Photoelectronic Thin Film Devices and Technology of Tianjin, Tianjin, 300350, PR China

^e Haihe Laboratory of Sustainable Chemical Transformations, Tianjin, 300192, PR China

^f Engineering Research Center of Thin Film Photoelectronic Technology of Ministry of Education, Tianjin, 300350, PR China

^g Collaborative Innovation Center of Chemical Science and Engineering (Tianjin), Tianjin, 300072, PR China

^h Jinneng Clean Energy Technology Ltd, Lvliang, Shanxi, 032100, PR China

A B S T R A C T

Benefiting from the effective passivated contacts, silicon heterojunction (SHJ) solar cells exhibit higher efficiency advantages compared to various crystalline silicon (c-Si) cell process routes. However, the large-scale production of SHJ cells is limited by the scarcity of indium-based Transparent Conductive Oxide (TCO) materials. To address this limitation, this study aims to prepare SHJ cells with less Indium Tin Oxide (ITO) consumption while maintaining performance (ITO-less cells). In particular, the material properties of ITO films with varying thickness was investigated and the impact of the silicon thin-film substrate on the growth mechanism of the ITO films and contact resistance was analyzed. By employing *n*-type nanocrystalline silicon (*n*-nc-Si:H) with a high crystallinity, the series resistance of ITO-less SHJ cells was minimized. Moreover, the incorporation of a LiF_x anti-reflection layer led to the successful fabrication of an ITO-less cell with a photoelectric conversion efficiency (PCE) of 21.28 %, consequently reducing ITO consumption by 75 %. These findings contribute to advancing the industrial-scale implementation of SHJ solar cells.

1. Introduction

The effective passivation contacts have enabled silicon heterojunction (SHJ) solar cells to achieve better performance compared to diffused junction cells, appears in a high open-circuit voltage (V_{oc}) surpassing 750 mV and a superior fill factor (FF). For bifacial contact SHJ solar cells, an impressive power conversion efficiency (PCE) of 26.81 % has been demonstrated on large-scale industrial-size (M6, 274.4 cm²) silicon wafer [1]. In contrast to the prevailing PERC cells in the market, SHJ cells offer several advantages, including elevated conversion efficiency, high bifaciality, and a simplified manufacturing process. Currently, the average PCE of PERC cell modules which dominate the market were around 20 %. However, research anticipate that by

2025, the average module efficiency of cells based on passivated contacts will exceed 22 % [2]. This expected improvement in efficiency holds great significance in reducing the levelized cost of electricity (LCOE). Despite these advantages, SHJ cells require transparent conductive oxide (TCO) to achieve both high light transmittance and efficient lateral carrier transport. Regrettably, the most widely used TCO materials for SHJ cells predominantly rely on Indium (In)-based oxides, and the scarcity of In reserves coupled with its high cost poses significant obstacles to the large-scale industrialization of SHJ solar cells.

Recent research efforts have been directed towards two main approaches to minimize the utilization of Indium in SHJ cells. The first approach involves exploring In-free TCO materials, such as zinc oxide-based [3–5] or tin oxide-based [6,7] TCO materials. The research

* Corresponding author. Institute of Photoelectronic Thin Film Devices and Technology, State Key Laboratory of Photovoltaic Materials and Cells, Nankai University, Tianjin, 300350, PR China.

** Corresponding author. Institute of Photoelectronic Thin Film Devices and Technology, State Key Laboratory of Photovoltaic Materials and Cells, Nankai University, Tianjin, 300350, PR China.

E-mail addresses: zhaoygd@nankai.edu.cn (Y. Zhao), xdzhang@nankai.edu.cn (X. Zhang).

¹ These authors contributed equally to this work.

focus is on improving the TCO and doped layer. The second is to reduce the amount of TCO, and develop a SHJ cell structure with less or no TCO. The focus is to reduce the photoelectric loss caused by the reduction of TCO. For the first route, Wu et al. utilized AZO instead of ITO to design a *p*-type a-Si:H/AZO contact with low contact resistance, which is similar to the cell efficiency using traditional ITO [4]. Wang et al. utilized the structure of ITO 50% /AZO 50% on the rear side of the cell, and the PCE loss was only 0.1% compared to pure ITO [5]. As for the second route, Han et al. utilized 25 nm tungsten-doped indium oxide (IWO) and 25 nm tin-doped indium oxide (ITO) for *n*-contact and *p*-contact respectively, which reduced the contact resistivity and obtained a PCE of more than 22% SHJ solar cells, the TCO consumption is reduced by 67% [8]. Gageot et al. utilized an ITO/SiN:H double-layer antireflective coating allowed for an SHJ cell with 15 nm-thick front ITO to achieve a PCE exceeding 22%, while also demonstrating that nc-Si:H exhibits better UV stability than nc-SiO_x:H, providing valuable insights for the development of ITO-less cells [9]. Cruz et al. proposed SiO₂ as the double-sided anti-reflection layer of SHJ cells to make up for the anti-reflection loss caused by thinning TCO. Using double-sided 20 nm TCO obtained a PCE of 24.6% similar to that of the 75 nm TCO reference cell, and the TCO consumption was reduced by 73% [10]. On the other hand, Li et al. completely removed the TCO of the light incident surface of the SHJ cell, and used ozone treatment to reduce the passivation quality caused by the direct contact between the metal and the amorphous silicon, and obtained a photoelectric conversion efficiency of >22% [11]. He et al. further utilized alkali metal fluoride/aluminum as the electron selective contact and transition metal oxide/silver as the hole selective contact, which reduced the contact resistance, and the PCE of the prepared full TCO-free cells exceeded 22.9% [12].

According to the analysis of existing technical routes, TCO-less cells can minimize the usage of indium oxide-based TCO without affecting PCE, and the implementation method is simple, which has greater industrialization prospects. Based on this, this study focuses on the material properties of ITO films with different thicknesses, and analyzes the influence of nc-Si:H on the growth of ITO, optimizes the contact characteristics of nc-Si:H/thinned ITO, and finally obtains a PCE of 21.28%. ITO-less SHJ solar cells, ITO usage is reduced by 75%.

2. Experiment details

FZ *n*-type c-Si wafers with a <100> crystalline plane orientation, a thickness of 180 μm, and a resistivity of 3–5 Ω cm² were utilized for the texturing process in a 1% KOH solution. Alcohols were employed as additives during the texturing procedure. Subsequently, the textured c-Si wafers under standard RCA cleaning, followed by a treatment with 1% HF to eliminate the oxide layer. The wafers were then loaded into a plasma-enhanced chemical vapor deposition (PECVD) system to deposit the passivation and carrier transport layers. Double-sided *i*-a-Si:H passivation layers were deposited, along with an *n*-a-Si:H (or *n*-nc-Si:H) electron transport layer on one side and a *p*-nc-Si:H hole transport layer on the other side, within the PECVD system. Table 1 presents the parameters employed in PECVD processes. ITO films with different thicknesses were deposited by thermal evaporation, followed by the deposition of a silver electrode. Finally deposited LiF_x thin films by thermal evaporation.

Table 1
PECVD system parameters for silicon thin films.

Sample	T _{dep} (°C)	Power Density (mW/cm ²)	Pressure (Torr)	SiH ₄ (sccm)	H ₂ (sccm)	1% B ₂ H ₆ (sccm)	1% PH ₃ (sccm)	CO ₂ (sccm)
<i>i</i> -a-Si: H	150	19	1.0	20	60	/	/	/
<i>n</i> -a-Si: H	180	36	1.3	4	100	/	4	/
Low χ _C <i>n</i> -nc-Si: H	180	54	1.3	3	180	/	1	/
High χ _C <i>n</i> -nc-Si: H	180	72	1.3	3	240	/	1	/
Seed layer	180	72	1.3	2	240	/	0.8	/
<i>p</i> -nc-Si:H	180	72	1.3	4	480	1	/	/

The film thickness was determined using a surface profilometer. The vertical resistance curve was measured using a Keithley 2400. The carrier mobility and carrier concentration of ITO samples on glass were measured by Ecopia HMS-7000 Hall effect measurement system. The refractive index and extinction coefficient of ITO samples on glass were extracted from the J.A. Woollam Co. RC2 ellipsometer measurements by fitting to a Tauc-Lorentz model. The reflectance and transmittance of ITO samples on glass were measured by Varian Cary 5000 spectrophotometer. The sheet resistance (R_{sheet}) of the ITO film on flat silicon wafer was measured using an RTS-5 four-point probe system. The contact resistance (ρ_C) was calculated by Cox & Strack method [13,14]. The test structure employed was Ag/ITO/*n*-nc-Si:H/*i*-a-Si:H/*n*-c-Si/*i*-a-Si:H/*n*-a-Si:H/ITO/Ag, where the Ag electrode on the *n*-a-Si:H side is fully covered. Seven disc electrodes with different areas (0.1 cm², 0.045 cm², 0.0314 cm², 0.0254 cm², 0.02 cm², 0.0113 cm², and 0.0078 cm²) were utilized on the *n*-nc-Si:H side. The Raman spectra of the materials on glass were measured by a Renishaw inVa Raman system with a laser wavelength of 532 nm to evaluate the crystallinity. For performance characterization, the current density-voltage (*J*-*V*) curve of the solar cells under standard conditions (AM1.5, 25 °C, 100 mW/cm²) was measured by a dual-light source solar simulator (Wacom Class AAA). The external quantum efficiency (EQE) was measured by a PV Measurement QEX10 system.

3. Results and discussion

3.1. Material properties of different thickness ITO

The photoelectric properties of ITO materials are mainly controlled by its doping concentration, grain size and content of oxygen vacancies [15–17]. Therefore, the influence of thinning ITO on its material properties should be considered first. Fig. 1(a) shows parameters such as resistivity, mobility, and carrier concentration of ITO with different thicknesses. It is evident that when the thickness of the ITO layer is ~10 nm, the resistivity becomes excessively high, with a significant reduction in both mobility and carrier concentration. Consequently, it becomes challenging to meet the requirements for efficient carrier transport. As the thickness of the ITO increases, the electrical properties of the material improve significantly. This is because achieving an adequate doping concentration and the formation of a stable cubic crystal phase require a certain degree of vertical growth. When the thickness of the ITO layer reaches 30 nm, the material exhibits a resistivity of 1.01 × 10⁻³ Ω·cm, a mobility of 32.66 cm²/V·s, and a carrier concentration of 1.9 × 10²⁰ cm⁻³. These properties essentially fulfill the requirements for carrier transport in SHJ cells. As the thickness of the ITO layer increases beyond 60 nm, its influence on the electrical properties tends to be saturated. Fig. 1(b) presents the XRD spectra of ITO films with varying thicknesses. As the thickness increases, the intensity of the diffraction peaks exhibits an upward trend, indicating an enhancement in crystallization. Additionally, the half-width of the diffraction peak at 2θ = 30.5° decreases, signifying an increase in grain size. Moreover, the increase in thickness also enhances the preferential growth tendency of the film along the (222) crystallographic orientation. It is generally accepted that ITO films with a (222) preferred orientation exhibit higher transmittance, carrier mobility, and doping

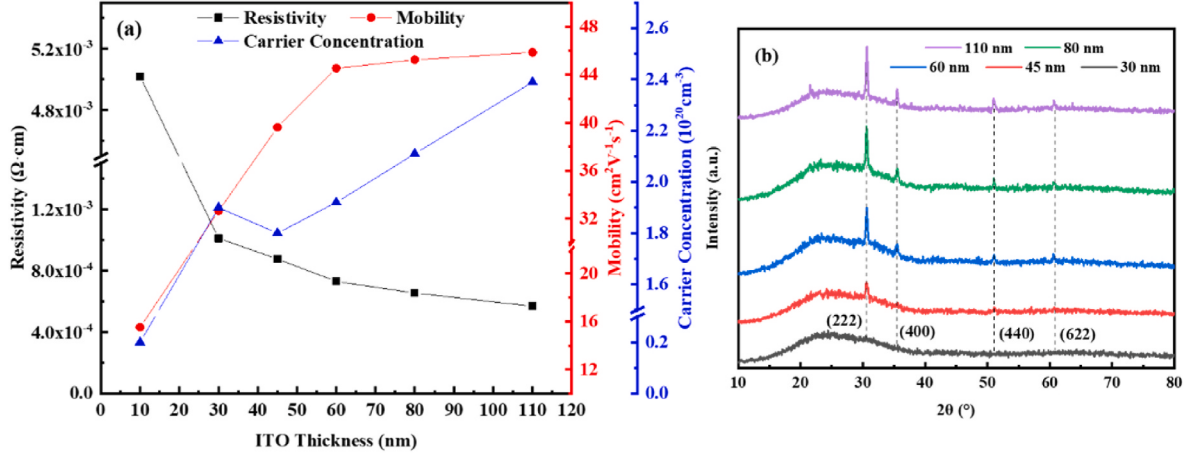


Fig. 1. (a) Resistivity, mobility and carrier concentration and (b) XRD spectra of ITO with varying thickness.

concentration [15,21]. Therefore, when designing ITO-less solar cells, the impact of reduced thickness on the electrical properties of ITO must be carefully considered.

The influence of ITO thickness on the optical properties of materials is also worth studying. Fig. 2 shows the reflectivity, transmittance, absorption coefficient, optical bandgap, and parameters such as refractive index and extinction coefficient for ITO of varying thicknesses. Fig. 2(a) shows that as the ITO thickness decreases from 110 nm to 30 nm, the transmittance of the film decreases while the reflectance increases within the wavelength range of 300–500 nm. This phenomenon is

attributed to the refractive index mismatch or interference effects variation induced by the thinning of the ITO layer, which reduces the antireflection efficiency. For wavelengths greater than 500 nm, the transmittance significantly increases as the film thickness decreases. This is attributed to the reduced free carrier absorption of long-wavelength photons caused by the thinning of the ITO layer. It is worth mentioning that a measurement artifact is observed at 800 nm in part of the spectrum in Fig. 2(a), which results from the switching of the light source. However, this does not impact the overall conclusions of the experiment. Fig. 2(b) illustrates the reduction in long-

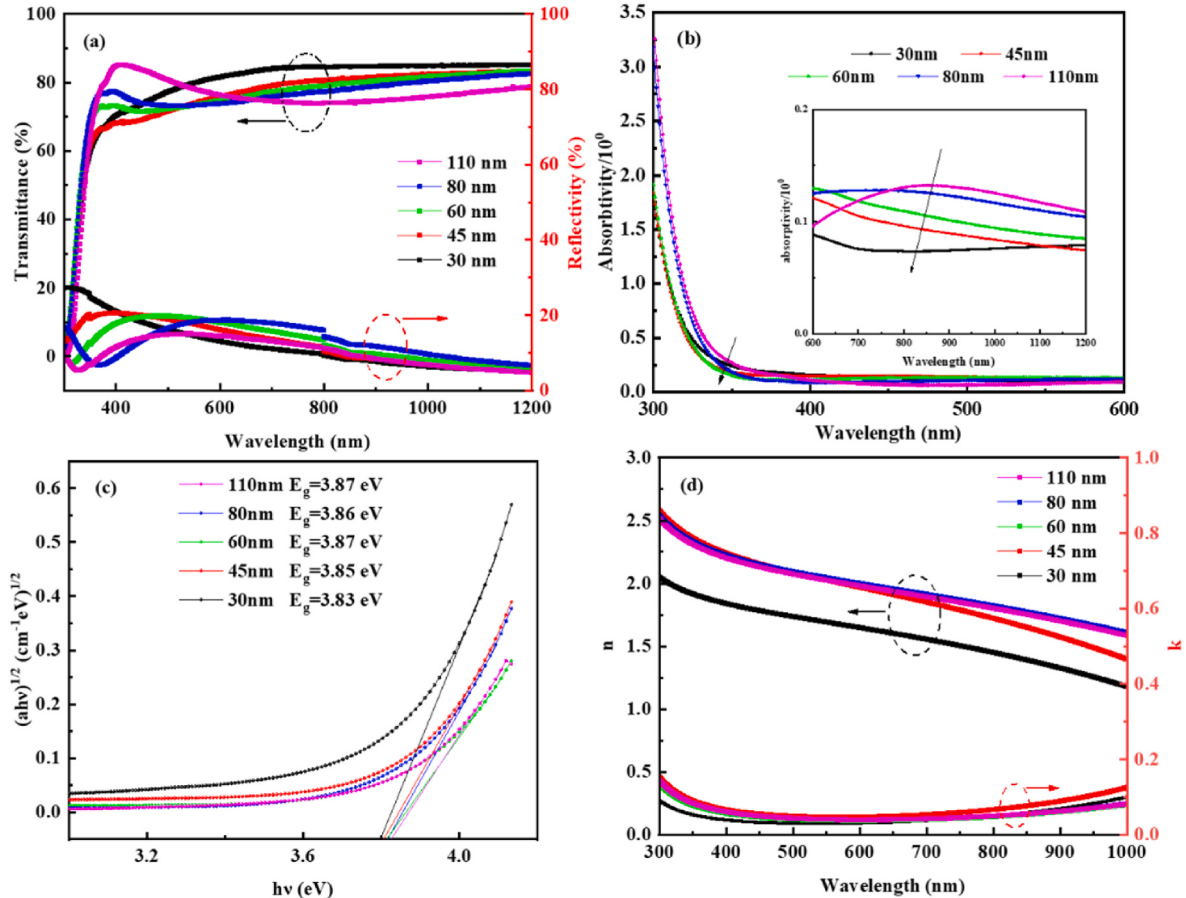


Fig. 2. (a) Transmittance and Reflectivity (b) Absorptivity (c) Optical bandgap and (d) Refractive index(n) and extinction coefficient(k) of ITO with varying thickness.

wavelength absorption as the ITO thickness decreases, which further supports the behavior observed at long-wavelength region in Fig. 2(a). Fig. 2(c) displays the optical bandgap of ITO films with varying thicknesses, showing a slight decrease in the optical bandgap as the film thickness is reduced. This phenomenon is attributed to the Moss-Burstein effect [18,19], where the reduction in film thickness leads to insufficient doping concentration, causing the Fermi level to shift towards the forbidden gap, which consequently reduces the optical band gap. Fig. 2(d) illustrates the refractive index (n) and extinction coefficient (k) of ITO as a function of thickness. When the ITO thickness exceeds 60 nm, both n and k remain relatively unaffected by further thinning. However, as the thickness decreases to 30 nm, $n@633$ nm declines from approximately 2.0 to 1.7. This will result in a refractive index mismatch in SHJ solar cells [20], thereby compromising the antireflection performance. Based on the aforementioned analysis, the potential degradation of optical performance resulting from ITO thinning in SHJ solar cells is primarily attributed to the insufficient antireflection effect. Consequently, when designing ITO-less structures, it is essential to implement additional strategies to compensate for the loss of antireflection performance.

3.2. Influence of silicon thin film substrate on ITO

In the SHJ cell, n/p -doped silicon film act as the selective contact layer, which also serves as the substrate for the ITO layer. This substrate has a substantial impact on the growth characteristics and material properties of ITO during the initial stages of deposition. Particularly at lower ITO thicknesses, the influence of the substrate on the material becomes more pronounced. Fig. 3 shows the SEM images of ITO deposited at different thicknesses on n -type doped silicon film substrates with varying crystallinity. In this experiment, the crystallinity for low χ_c n -nc-Si: H is approximately 25 %, while for high χ_c n -nc-Si: H is approximately 60 %. Fig. 3(a)–(c) show the SEM images of n -doped silicon films with varying crystallinity. Notably, the film with high crystallinity exhibits a well-defined grain structure. Fig. 3(d)–(f) correspond to 30 nm-thick ITO films grown on n -doped silicon films with

varying crystallinity. Similar to single-layer silicon films, the surface of ITO grown on silicon films with high crystallinity has a more obvious grain structure. Fig. 3(g)–(i) shows the growth of 110 nm ITO films on silicon films with varying crystallinity and the surface morphology of this group of samples tends to be similar. Based on the aforementioned morphological characteristics, it can be inferred that the initial state of ITO growing on the surface of the silicon film is related to the crystallization state of the silicon film itself, and the silicon film substrate with high crystallinity can promote the rapid crystallization of ITO, thereby obtaining a more complete grain structure at lower thicknesses. However, due to the sufficient vertical growth dimension of high-thickness ITO, exhibits a reduced correlation between the surface morphology and the substrate. The XRD spectra in Fig. S1 further corroborates the aforementioned conclusion. The mobility of ITO is related to its degree of grain boundary scattering [21,22]. High-mobility ITO materials require reduced grain boundary scattering; therefore, it is necessary to increase the grain size to achieve ITO films with high photoelectric performance. For thin ITO films, utilizing a substrate with a high crystallinity is an effective approach to facilitate rapid crystallization.

The contact resistance (ρ_C) between silicon film and ITO is a key factor influencing the series resistance (R_{series}) in SHJ solar cells. Considering the degradation of electrical properties due to the thinning of ITO, it is crucial to account for the impact of varying ITO thicknesses on ρ_C . Fig. 4 shows the ρ_C between n -type doped silicon thin films of varying crystallinity and ITO layers of different thicknesses. The statistical results indicate that when the ITO thickness is higher, the ρ_C between ITO and n -type doped silicon film is directly proportional to the crystallinity of the n -type doped silicon film. Conversely, when the ITO thickness is lower, the ρ_C becomes inversely proportional to the crystallinity of the n -type doped silicon film. This is attributed to the differences in the behavior of ITO on different substrates such as crystal growth and hydrogen diffusion. The research presented in the previous section demonstrates that thin ITO films grown on substrates with silicon thin films of high crystallinity exhibit enhanced crystalline degree, which reduces grain boundary scattering, thereby improving carrier mobility. In the case of thick ITO films, Cruz et al. observed a higher

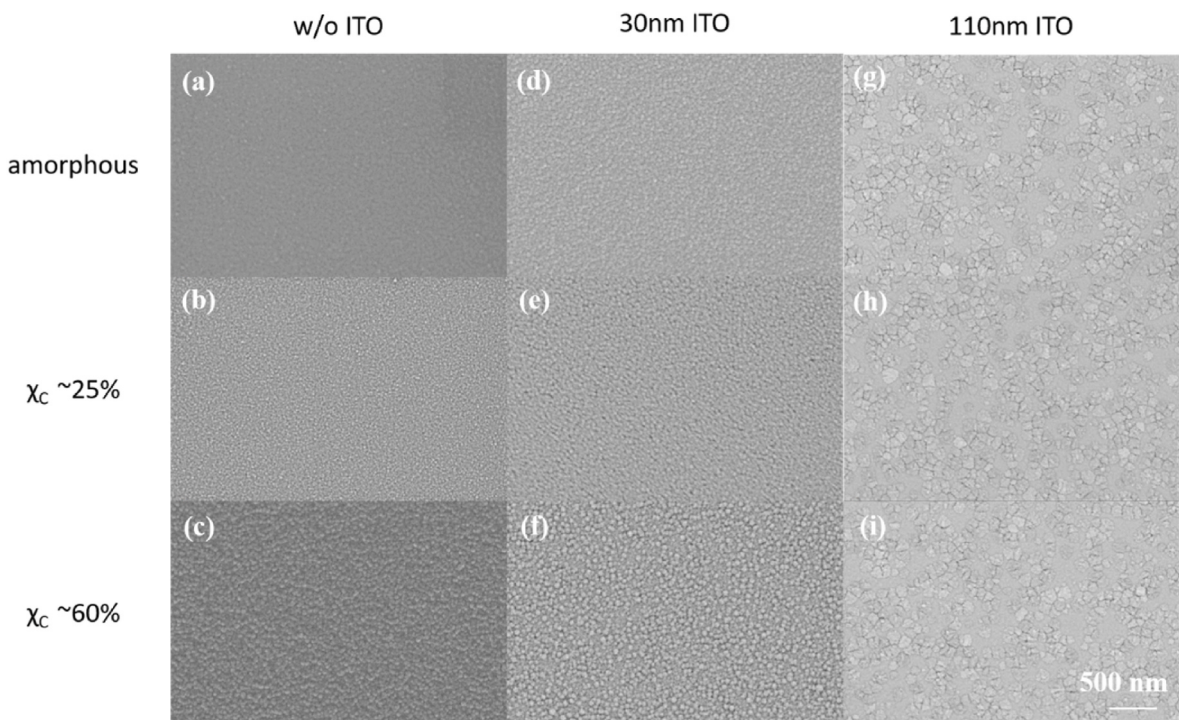


Fig. 3. SEM images of (a)–(c) n -doped silicon films with varying crystallinity (d)–(f) 30 nm ITO films deposited on n -doped silicon films with varying crystallinity (g)–(i) 110 nm ITO films deposited on n -doped silicon films with varying crystallinity.

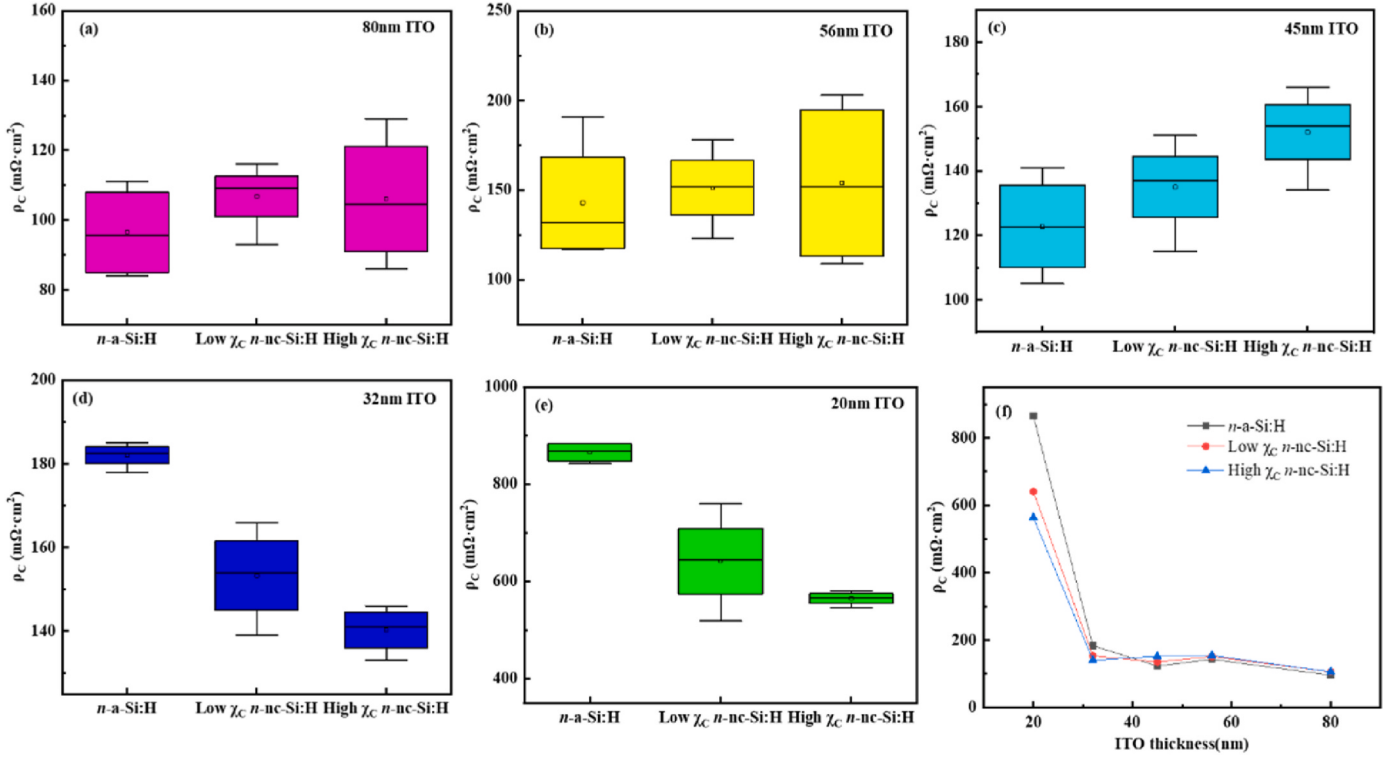


Fig. 4. The contact resistance (ρ_c) between *n*-type doped silicon thin films of varying crystallinity and ITO layers of different thicknesses: (a) 80 nm (b) 56 nm (c) 45 nm (d) 32 nm (e) 20 nm, and (f) statistical chart of the mean values. (For interpretation of the references to colour in this figure legend, the reader is referred to the Web version of this article.)

prevalence of small grain structures within the 100 nm-thick ITO film grown on a nc-Si: H silicon substrate, which is attributed to crystal fracture and subsequent recrystallization [22]. As a result, ITO grown on nc-Si exhibits a smaller average particle size compared to ITO grown on a-Si. Moreover, nc-Si: H significantly inhibits hydrogen diffusion during annealing to a greater extent than a-Si: H, leading to insufficient hydrogenation of the ITO film [23]. The aforementioned two factors contribute to the reduced mobility of thick ITO deposited on a silicon thin-film substrate with a high crystallinity, which consequently higher ρ_c .

3.3. Preparation of ITO-less SHJ solar cells

The established SHJ solar cell technology employs *n*-a-Si:H as the electron transport layer on the light-incident side. Fig. 5 shows the *J-V* and EQE curves of the cell after thinning ITO on the electron transport layer based on *n*-a-Si:H, while maintaining a constant thickness of 110 nm for the rear ITO layer. As shown in Fig. 5(a), when the thickness of the ITO layer on the light-incident side decreases from 80 nm to 20 nm, the V_{oc} of the cell remains nearly unchanged, while the J_{sc} gradually decreases. The FF initially exhibits minimal variation, but gradually decreases as the ITO thickness is further reduced (refer to Table S1). The observed trend in J_{sc} is attributed to the reduction in ITO thickness,

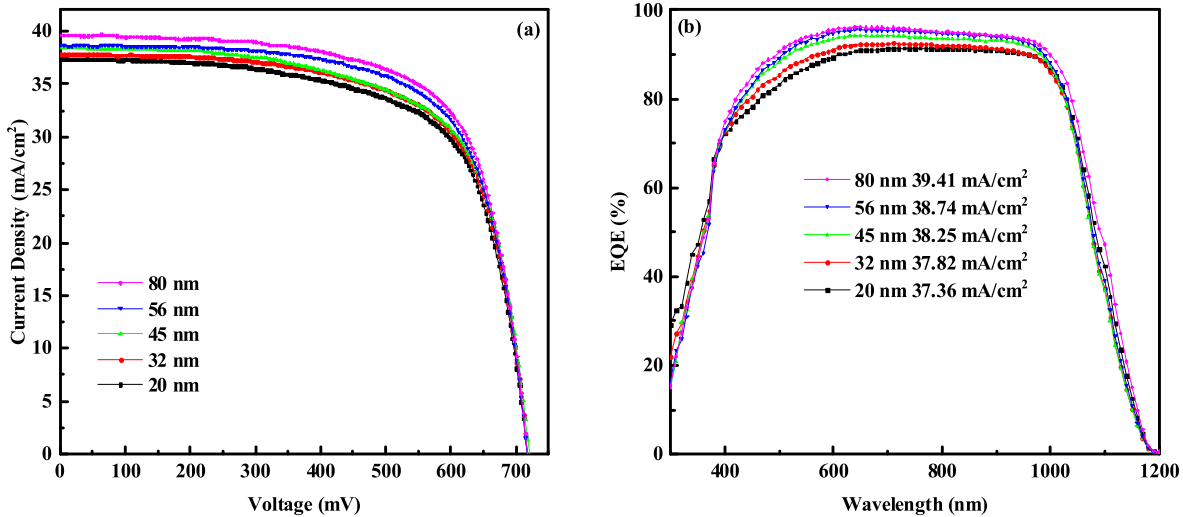


Fig. 5. (a) *J-V* and (b) EQE curves of SHJ solar cells with varying ITO thicknesses on the light-incident side. (Detailed cell parameters refer to Table S1.).

which reduces the anti-reflection effect and results in significant light losses at the front surface. As shown in the EQE curve of Fig. 5(b), the optical losses are most pronounced in the 400–600 nm wavelength range. The decrease in FF is primarily due to the increase in R_{series} , which results from the rise in ρ_C as well as R_{sheet} following the thinning of the ITO layer, as shown in Fig. 4 and Fig. S2.

To further reduce the usage of ITO in SHJ cells, the effect of reducing the rear-side ITO thickness on cell performance was investigated, while maintaining the front-side ITO thickness at 80 nm. Fig. 6 shows the J-V and EQE curves of the SHJ cells, in which the thickness of the rear-side ITO layer has been reduced from 80 nm to 20 nm. It can be observed that the V_{OC} is minimally impacted by the ITO thickness, while J_{SC} experiences a slight reduction of 0.35 mA/cm^2 , and the FF decreases from 69.05 % to 68.24 %. In comparison to the thinning of the front-side ITO, reducing the thickness of the rear-side ITO causes less degradation to the device parameters. This is primarily due to two factors: a) From an optical perspective, the requirement for the rear-side ITO's anti-reflection effect is lower than that of the front-side ITO due to the presence of a full-area silver electrode; b) From an electrical perspective, due to the utilization of a full-area silver electrode on the rear side, the demand for lateral carrier transport in the rear ITO is also less critical compared to the front-side ITO. Based on the above analysis, further optimization of the front-side ITO thinning process is essential to enhance the performance of ITO-less solar cells.

The experiments in Section 3.2 have demonstrated that for ITO-less structures, substituting $n\text{-a-Si:H}$ with $n\text{-nc-Si:H}$ can reduce the ρ_C between n -type silicon film and thin ITO. Fig. 7(a) shows the J-V curves of SHJ cells of n -doped silicon films with varying crystallinity, measured under a front ITO layer thickness of 20 nm. The elevated crystallinity of $n\text{-nc-Si:H}$ notably enhances the PCE of SHJ solar cell, primarily attributed to the reduction in R_{series} , which aligns with the observed decrease in ρ_C . To further minimize the R_{series} of the cell, a seed layer was incorporated, and the thickness of the $n\text{-nc-Si:H}$ layer was optimized, the schematic diagram of the cell structure is shown in Fig. 7(b). Fig. 7(c)–(f) present the statistical graphs of the cell parameters for $n\text{-nc-Si:H}$ layers with thicknesses ranging from 4 to 8 nm. There is a certain longitudinal microstructure evolution in the growth of microcrystals within $n\text{-nc-Si:H}$. For $n\text{-nc-Si:H}$ layers with a thickness of 4 nm, both crystallinity and doping efficiency are low, which limits carrier transport and reduces field-effect passivation. These lead to losses in both V_{OC} and FF. As the thickness of the $n\text{-nc-Si:H}$ layer increases to 6 nm, both the field-effect passivation and carrier transport properties are enhanced, resulting in simultaneous improvements in V_{OC} and FF. As the thickness

of the $n\text{-nc-Si:H}$ layer is further increased to 8 nm, carrier transport losses and parasitic absorption both increases, leading to a reduction in J_{SC} and FF. Based on the above analysis, the optimal cell efficiency of 19.75 % is achieved when the n -type doped layer combines a seed layer with a 6 nm $n\text{-nc-Si:H}$ layer, yielding $V_{\text{OC}} = 729.4 \text{ mV}$, $J_{\text{SC}} = 37.32 \text{ mA/cm}^2$, and FF = 72.55 %. Compared to the reference cell (80 nm ITO in Table S1), both V_{OC} and FF show improvements. However, there remains a loss in J_{SC} , which is attributed to an insufficient anti-reflection effect.

To compensate for the loss of front-side anti-reflection due to the reduced ITO thickness, an anti-reflection layer with a refractive index between that of air and ITO is applied to the ITO surface. This creates a refractive index gradient, effectively minimizing the loss of incident light on the front surface of the cell [24]. Lithium fluoride (LiF_x), with a refractive index of around 1.4, is commonly used as an anti-reflection layer in SHJ cells. To optimize the balance between anti-reflection effects and transmission performance, the impact of varying LiF_x thicknesses on cell performance was evaluated, as illustrated in Fig. 8(a)–(b). The optimal PCE is achieved when the LiF_x thickness is approximately 90 nm, at which the spectral response of the EQE reaches its maximum. The incorporation of a 90 nm anti-reflection layer results in a J_{SC} gain of approximately 2 mA/cm^2 compared to the cell without the LiF_x anti-reflection layer. Finally, employing the structure illustrated in Fig. 8(c), the ITO on both sides of the SHJ cell was reduced to 20 nm, and a 90 nm LiF_x anti-reflection layer was applied to the incident light surface. The champion PCE of the ITO-less cell is 21.28 %, with $V_{\text{OC}} = 738.7 \text{ mV}$, $J_{\text{SC}} = 39.32 \text{ mA/cm}^2$ and FF = 73.28 %. Compared to standard SHJ cells (refers to Fig. S3), this configuration achieves a 75 % reduction in ITO usage, while the PCE loss is only $-0.47\%_{\text{abs}}$.

4. Conclusion

In conclusion, this study aims to develop ITO-less silicon heterojunction solar cells. To achieve this objective, the impact of ITO thinning on material properties was investigated, followed by an analysis of the variations in the growth mechanisms of ITO on different substrates. Based on theoretical analysis and contact resistance measurements, the benefit of using $n\text{-nc-Si:H}$ substrates with a high crystallinity to reduce $n\text{/ITO}$ contact resistance has been quantified. The PCE of the ITO-less cell is enhanced through the application of a seed layer and optimization of the $n\text{-nc-Si:H}$ layer thickness. Finally, a LiF_x anti-reflection coating is applied to compensate for the optical losses resulting from ITO thinning. The champion PCE achieved by the resulting ITO-less cell

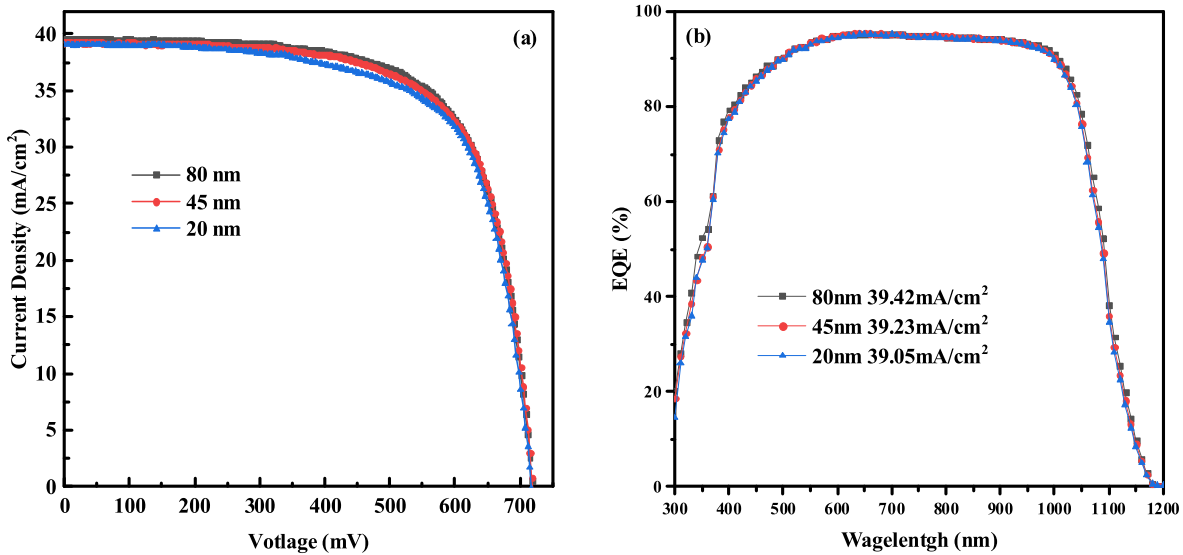


Fig. 6. (a) J-V and (b) EQE curves of SHJ solar cells with varying ITO thicknesses on the rear side (Detailed cell parameters refer to Table S2.).

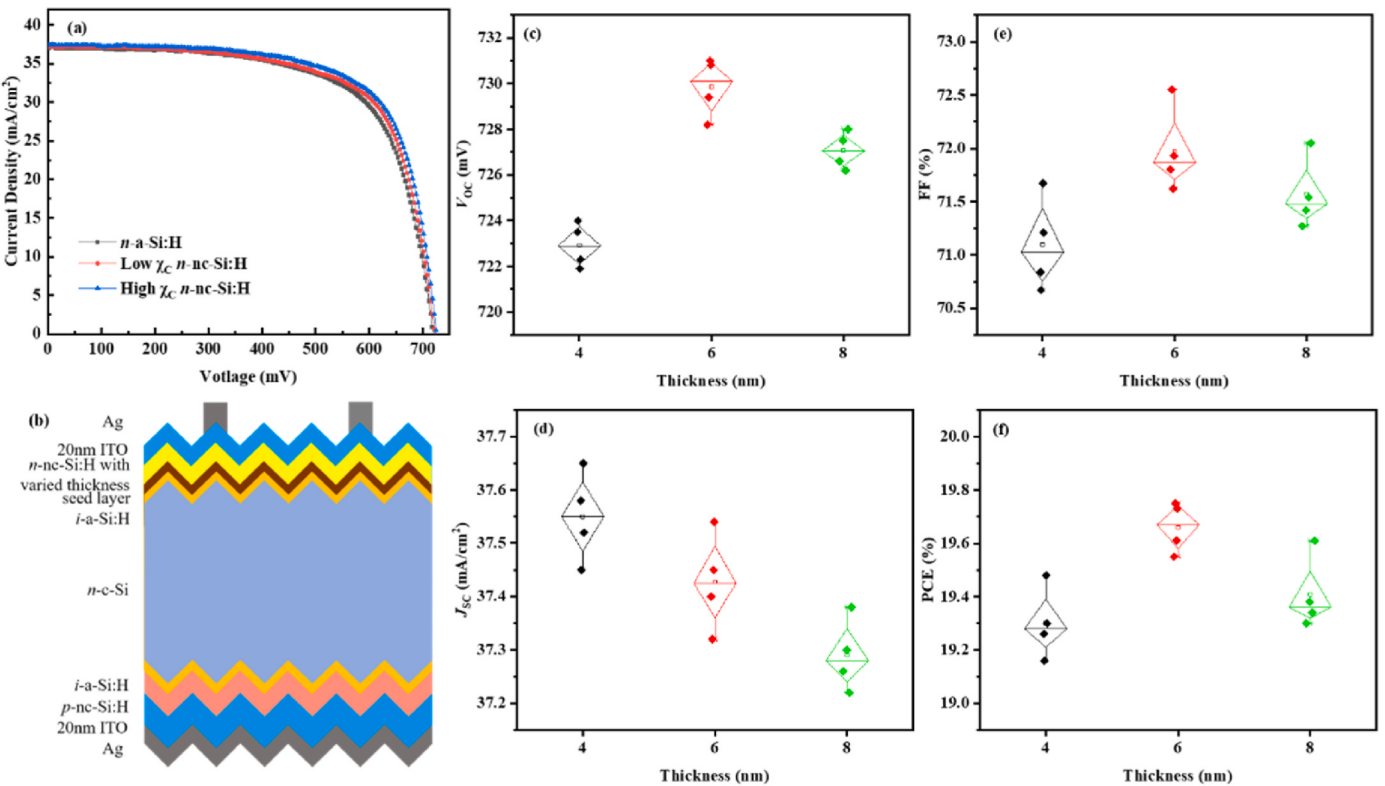


Fig. 7. (a) $J-V$ curves of ITO-less SHJ cells of n -doped silicon films with varying crystallinity (b) schematic diagram of cell structure and statistical graphs of (c) V_{oc} (d) J_{sc} (e) FF (f) PCE of SHJ cells with varying n -nc-Si:H thickness (Detailed cell parameters refer to Table S3.). (For interpretation of the references to colour in this figure legend, the reader is referred to the Web version of this article.)

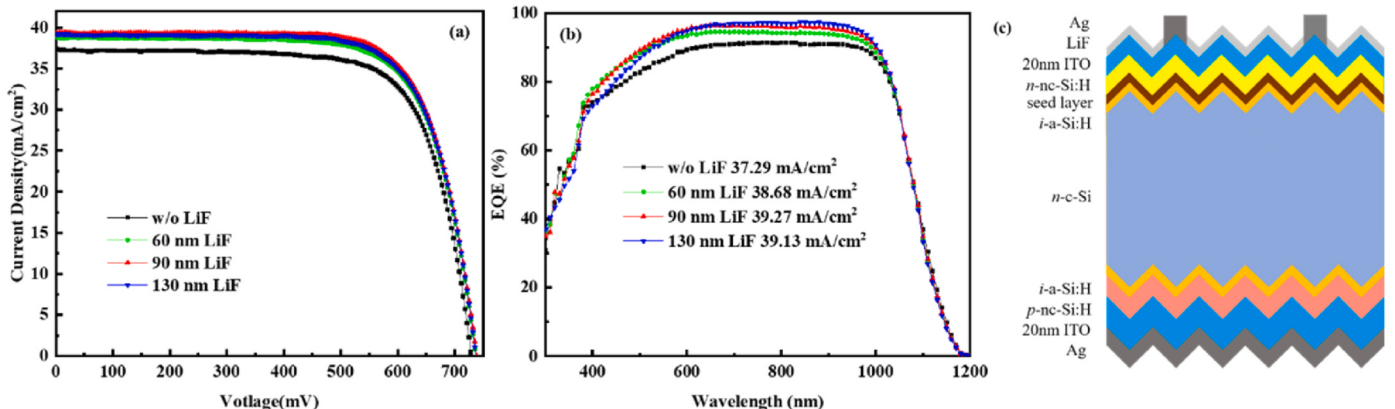


Fig. 8. (a) $J-V$ (b) EQE curves of ITO-less cells with varying LiF_x thickness (c) schematic diagram of ITO-less SHJ cell (Detailed cell parameters refer to Table S4.).

was 21.28 %, with a 75 % reduction in ITO usage.

CRediT authorship contribution statement

Yuxiang Li: Writing – original draft, Methodology, Investigation, Formal analysis, Conceptualization. **Yubo Zhang:** Methodology, Investigation, Formal analysis, Data curation. **Xuejiao Wang:** Methodology, Investigation. **Jilei Wang:** Resources. **Guanlan Chen:** Methodology, Investigation. **Biao Shi:** Methodology, Investigation. **Liyou Yang:** Resources. **Wenhong Wang:** Validation, Supervision. **Ying Zhao:** Supervision, Resources, Project administration, Funding acquisition. **Xiaodan Zhang:** Supervision, Resources, Project administration, Funding acquisition.

Declaration of competing interest

The authors declare no competing financial interest.

Acknowledgments

The authors are grateful for the financial support of the National Key Research and Development Program of China (Grant No. 2022YFB4200102), the Joint Funds of the National Natural Science Foundation of China (Grant No. U21A2072), the National Natural Science Foundation of China (Grant No. 62274099), the Overseas Expertise Introduction Project for Discipline Innovation of Higher Education of China (Grant No. B16027), Tianjin Science and Technology Project (Grant No. 18ZXJMTG00220), Key R&D Program of Hebei Province

(Grant No. 19214301D), Natural Science Foundation of Tianjin (Grant No. 20JCQNJC02070), China Postdoctoral Science Foundation (Grant No. 2020T130317), Financial support was provided by the Haihe Laboratory of Sustainable Chemical Transformations, and the Fundamental Research Funds for the Central Universities, Nankai University.

Appendix A. Supplementary data

Supplementary data to this article can be found online at <https://doi.org/10.1016/j.solmat.2025.113422>.

Data availability

Data will be made available on request.

References

- [1] H. Lin, M. Yang, X. Ru, et al., Silicon heterojunction solar cells with up to 26.81% efficiency achieved by electrically optimized nanocrystalline-silicon hole contact layers, *Nat. Energy* (2023) 1–11.
- [2] C. Ballif, F.J. Haug, M. Boccardi, et al., Status and perspectives of crystalline silicon photovoltaics in research and industry, *Nat. Rev. Mater.* 7 (8) (2022) 597–616.
- [3] Q. Tang, W. Duan, A. Lambertz, et al., 85% indium reduction for high-efficiency silicon heterojunction solar cells with aluminum-doped zinc oxide contacts, *Sol. Energy Mater. Sol. Cell.* 251 (2023) 112120.
- [4] Z. Wu, W. Duan, A. Lambertz, et al., Low-resistivity p-type a-Si: H/AZO hole contact in high-efficiency silicon heterojunction solar cells, *Appl. Surf. Sci.* 542 (2021) 148749.
- [5] J. Wang, C. Meng, H. Liu, et al., Application of indium tin oxide/aluminum-doped zinc oxide transparent conductive oxide stack films in silicon heterojunction solar cells, *ACS Appl. Energy Mater.* 4 (12) (2021) 13586–13592.
- [6] C. Yu, Q. Zou, Q. Wang, et al., Silicon solar cell with undoped tin oxide transparent electrode, *Nat. Energy* 8 (10) (2023) 1119–1125.
- [7] J. Guo, S. Li, Y. Cui, et al., Low-cost tin oxide transparent conductive films for silicon heterojunction solar cells, *Adv. Funct. Mater.* 34 (45) (2024) 2407273.
- [8] C. Han, R. Sanbergen, M. van Duffelen, et al., Towards bifacial silicon heterojunction solar cells with reduced TCO use, *Prog. Photovoltaics Res. Appl.* 30 (7) (2022) 750–762.
- [9] T. Gageot, J. Veirman, F. Jay, et al., Feasibility test of drastic indium cut down in SHJ solar cells and modules using ultra-thin ITO layers, *Sol. Energy Mater. Sol. Cell.* 261 (2023) 112512.
- [10] A. Cruz, D. Erfurt, P. Wagner, et al., Optoelectrical analysis of TCO+ Silicon oxide double layers at the front and rear side of silicon heterojunction solar cells, *Sol. Energy Mater. Sol. Cell.* 236 (2022) 111493.
- [11] S. Li, M. Pomaska, A. Lambertz, et al., Transparent-conductive-oxide-free front contacts for high-efficiency silicon heterojunction solar cells, *Joule* 5 (6) (2021) 1535–1547.
- [12] J. He, G. Wang, Y. Qiu, et al., Enabling transparent-conductive-oxide free efficient heterojunction solar cells by flexibly using dopant-free contact, *Adv. Funct. Mater.* 32 (39) (2022) 2205901.
- [13] R.H. Cox, H. Strack, Ohmic contacts for GaAs devices, *Solid State Electron.* 10 (12) (1967) 1213–1218.
- [14] W. Wang, H. Lin, Z. Yang, et al., An expanded Cox and Strack method for precise extraction of specific contact resistance of transition metal oxide/n-silicon heterojunction, *IEEE J. Photovoltaics* 9 (4) (2019) 1113–1120.
- [15] F. Kurdesau, G. Khrapunov, A.F. Da Cunha, et al., Comparative study of ITO layers deposited by DC and RF magnetron sputtering at room temperature, *J. Non-Cryst. Solids* 352 (9–20) (2006) 1466–1470.
- [16] U. Betz, M.K. Olsson, J. Marthy, et al., Thin films engineering of indium tin oxide: large area flat panel displays application, *Surf. Coating. Technol.* 200 (20–21) (2006) 5751–5759.
- [17] S. Elhalawaty, K. Sivaramakrishnan, N.D. Theodore, et al., The effect of sputtering pressure on electrical, optical and structure properties of indium tin oxide on glass, *Thin Solid Films* 518 (12) (2010) 3326–3331.
- [18] E. Burstein, Anomalous optical absorption limit in InSb, *Phys. Rev.* 93 (3) (1954) 632.
- [19] T.S. Moss, The interpretation of the properties of indium antimonide, *Proc. Phys. Soc. B* 67 (10) (1954) 775.
- [20] F. Meng, J. Shi, L. Shen, et al., Characterization of transparent conductive oxide films and their effect on amorphous/crystalline silicon heterojunction solar cells, *Jpn. J. Appl. Phys.* 56 (4S) (2017) 04CS09.
- [21] K. Ellmer, R. Mientus, Carrier transport in polycrystalline transparent conductive oxides: a comparative study of zinc oxide and indium oxide, *Thin Solid Films* 516 (14) (2008) 4620–4627.
- [22] C. Lohaus, C. Steinert, G. Deyu, et al., Enhancing electrical conductivity of room temperature deposited Sn-doped In2O3 thin films by hematite seed layers, *Appl. Phys. Lett.* 112 (15) (2018) 152105.
- [23] A. Cruz, F. Ruske, A. Eljarrat, et al., Influence of silicon layers on the growth of ITO and AZO in silicon heterojunction solar cells, *IEEE J. Photovoltaics* 10 (2) (2019) 703–709.
- [24] A.J. Addie, R.A. Ismail, M.A. Mohammed, Amorphous carbon nitride dual-function anti-reflection coating for crystalline silicon solar cells, *Sci. Rep.* 12 (1) (2022) 9902.